

pubs.acs.org/cm Article

# Control of Lithium Salt Partitioning, Coordination, and Solvation in Vitrimer Electrolytes

Seongon Jang, Erick I. Hernandez Alvarez, Chen Chen, Brian B. Jing, Chengtian Shen, Paul V. Braun, André Schleife, Charles M. Schroeder,\* and Christopher M. Evans\*



Cite This: Chem. Mater. 2023, 35, 8039-8049



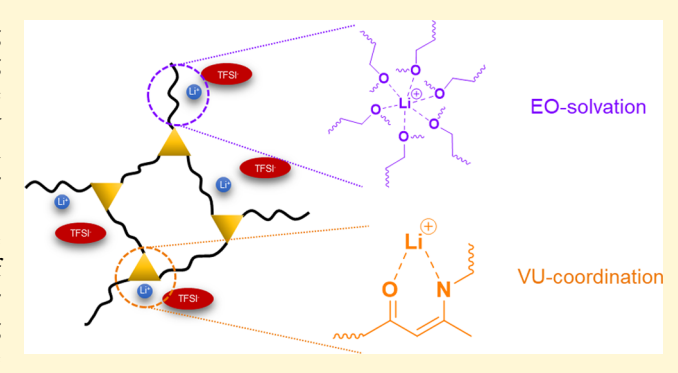
**ACCESS** I

Metrics & More

Article Recommendations

s Supporting Information

ABSTRACT: Vitrimers are an important class of materials offering advantages over conventional thermosets due to their self-healing properties and reprocessability. Vitrimers are ideal candidate materials for solid polymer electrolytes because their viscoelasticity and conductivity can be independently tuned by salt addition in distinct ways from linear polymer electrolytes while further providing resistance to lithium dendrite propagation. In this work, the chemical and physical properties of vinylogous urethane (VU) vitrimers were characterized by using a combination of experiments and simulations to develop molecular design rules for controlling material properties. A series of VU vitrimers containing lithium bis(trifluoromethanesulfonyl)imide (LiTFSI) salt were synthesized by precisely controlling the VU cross-linking density



using defined linker lengths of ethylene glycol (xEG, x =  $^2$ 2, 3, 4,  $^6$ 6, or 12), thereby enabling control over the dynamic bond-to-EG ratio. Viscoelastic measurements show that the characteristic relaxation time  $\tau^*$  of VU vitrimers containing salt decreased by a factor of  $\sim$ 70 relative to neutral vitrimers due to Li-ion coordination and catalysis of VU bond exchange. Stress relaxation times and shear moduli decrease with lower cross-linking densities in VU vitrimers. Solid-state  $^7$ Li NMR further reveals that VU vitrimers with longer linker lengths prefer lithium-ethylene oxide (Li-EO) solvation, whereas shorter linkers cannot sufficiently solvate the cation, and Li-VU coordination is preferred. Density functional theory (DFT) simulations were used to elucidate the dominant binding mode of Li-ion interaction as a function of linker length. The preferential partitioning of Li at the VU site leads to an order of magnitude decrease in stress relaxation times with a negligible impact on the conductivity after normalizing to the glass transition temperature  $T_g$ . Interestingly, our results show universal behavior for  $T_g$ -normalized ionic conductivity data regardless of linker length. Overall, this work provides new avenues for orthogonal tuning of bulk dynamics, recyclability, and conductivity in vitrimer electrolytes.

## INTRODUCTION

The worldwide demand for synthetic plastic materials continues to increase.1 Permanent polymer networks such as thermosets and elastomers are currently used for a wide range of applications due to their robust mechanical and thermal properties, as well as high chemical resistance. However, a major shortcoming of permanent networks is the inability to reprocess or recycle these materials after curing because their cross-links are composed of permanent covalent bonds.<sup>2</sup> To address these issues, significant efforts are currently focused on the design and development of new recyclable and sustainable polymeric materials to mitigate the generation of nondegradable polymer waste in the environment.<sup>3</sup> Covalent adaptable networks (CANs) are a class of polymer networks containing dynamic bonds that allow for flow and reprocessing, enabling access to recyclability. When the bonds exchange by an associative mechanism, these materials are typically referred to as "vitrimers". A CANs exhibit behavior on the spectrum between thermosets to thermoplastics depending on the crosslink density, exchange kinetics, and polymer backbone.<sup>5,6</sup> In recent years, vitrimers have been considered for various applications including 3D printing, self-healing materials,<sup>7,8</sup> shape-memory materials,<sup>9–11</sup> composites,<sup>12–15</sup> shockwave dissipation,<sup>16</sup> and solid polymer electrolytes.<sup>17–24</sup>

Solid-state electrolytes have been investigated extensively as potentially safer alternatives to flammable and toxic liquid electrolytes and exhibit good interfacial contact with electrodes. Poly(ethylene oxide) (PEO) is a common chemical motif known to facilitate lithium ion transport by ion coordination with the backbone ether oxygens. Although PEO-based polymer electrolytes show high ionic conductiv-

Received: June 1, 2023

Revised: September 12, 2023 Published: September 28, 2023





ity, 39,40 these materials exhibit relatively low conductivity at room temperature and a strong temperature-dependent modulus that drops substantially upon heating. 41-44 To enhance their mechanical properties, PEO can be covalently or noncovalently cross-linked, leading to rubbery electrolytes (characteristic plateau modulus ~0.1 MPa) with suppressed dendrite formation due to the nanoscale mesh size in crosslinked PEO. 45,46,68 However, covalent permanent networks are not easily reprocessed or recycled after the curing processes. In recent years, vitrimers have received increased attention as robust and recyclable solid polymer electrolytes. <sup>17–24</sup> Various dynamic bonds such as boronic ester, <sup>23,24,71,80</sup> imine, <sup>19–21,77,78</sup> vinylogous urethane, <sup>22</sup> boroxine, <sup>79</sup> and disulfide <sup>69,70,74–76</sup> have been previously incorporated into vitrimers for solid-state electrolyte applications. Soy protein-based imine (SPI) dynamic networks were prepared by the Fang group." This malleable vitrimer can be recycled at ambient temperature (25 °C), which could facilitate the sustainable processing of solid polymer electrolytes. Yang and co-workers demonstrated both excellent cell performance and improved cycle stability up to 1800 h using epoxy resin backbones and reversible disulfide cross-linking. 14 The Meng group incorporated double dynamic bonds into solid polymer electrolytes, demonstrating improved self-healing abilities and high ionic conductivity at 30 °C. Furthermore, dynamic boroxine and imine polymer electrolytes possess good interfacial stability with lithium metal anodes, which can effectively suppress Li dendrite formation. Bao and co-workers demonstrated the direct reprocessing of dynamic polymer network electrolytes using vinylogous urethane (VU) chemistry without detrimental loss of mechanical and ion transport performance,<sup>22</sup> showing that the addition of lithium salts accelerates dynamic exchange and that network dynamics can be tuned by changing the amount of excess amine. However, the mechanism of Li-ion partitioning between VU bonds and the EO backbones is unknown, and the impact of ion coordination on the conductivity, reprocessability, and complex viscoelasticity of vitrimer electrolytes is not well understood.

VU bonds can be thermally activated without a catalyst,<sup>25</sup> with dynamic bond exchange occurring catalyst-free at temperatures above 130 °C. In addition, VU vitrimers exhibit a storage modulus of around 2.4 GPa at operable temperatures, and these materials can be recycled multiple times by hot compression molding without significant loss of mechanical properties. Prior work has shown that the viscoelastic behavior of VU networks can be controlled by the addition of acid, base, or Lewis acids.<sup>27</sup> In neutral or acidic conditions, the amine exchange occurs through an iminium pathway. However, in the presence of a strong base, proton exchange is prohibited, and the amine exchange occurs through a direct Michael addition pathway. Recently, the effect of nonstoichiometric balance on the viscoelastic behavior of VU-based vitrimers was studied,<sup>26</sup> revealing that excess amounts of amine groups accelerate dynamic exchange, which leads to significant decreases in the characteristic stress relaxation times. Despite recent progress, however, the coordination and solvation of salts in VU vitrimers and the corresponding impact on conductivity are not fully understood.

In this work, we investigate how the partitioning of Li-ion coordination between VU bonds and ether oxygens in ethylene glycol linkers dictates the viscoelastic properties and ionic conductivity of vitrimers. A series of precise VU networks with varying ethylene glycol linker lengths and added Li salt were

synthesized. Rheological measurements show that the addition of salt accelerates the relaxation of the networks due to the catalytic effect of Li cations on dynamic bond exchange. <sup>7</sup>Li solid-state NMR indicates that Li cations coordinate with the VU moiety for short vitrimer linker lengths but preferentially coordinate in an EO environment for longer linkers. Our results show a universal dependence of ionic conductivity on temperature when normalized by the glass transition temperature  $T_g$  of VU vitrimers, suggesting that ion transport is primarily dominated by segmental dynamics regardless of cross-linking density. However, the addition of salts has a major impact on viscoelasticity and stress relaxation in Li-VU vitrimers. Finally, we demonstrate that salt can be used to reprocess and recycle VU vitrimers using a hot press without significant degradation. Overall, our results offer key new insights for controlling the properties of VU-based vitrimers through salt addition and cross-linking density, which could aid in the design and development of sustainable electrolytes.

#### **■** EXPERIMENTAL SECTION

**Materials.** Diethylene glycol (2EO, 99%), triethylene glycol (3EO, 99%), tetraethylene glycol (4EO, 99%), tert-butyl acetoacetate (tBA, 98%), propylamine (99%), lithium bis(trifluoromethanesulfonyl)-imide (LiTFSI, 99%), diethylene glycol ethyl ether (DEG, 99%), anhydrous tetrahydrofuran (THF, 99.9%), and anhydrous dichloromethane (CH $_2$ Cl $_2$ , 99.8%) were purchased from Sigma-Aldrich. Hexaethylene glycol (6EO, 99%) was purchased from AK Scientific. 3,6,9,12,15,18,21,24,27,30,33-Undecaoxapentatriacontane-1,35-diol (12EO, 97%) was purchased from Ambeed. Tris(2-aminoethyl)amine (TEA, 98%) was purchased from TCI America. Ethyl ether (anhydrous) and acetone (certified ACS) were purchased from Fisher Chemical. Purchased chemicals were used without further purification.

Synthetic Procedures. Acetylation of Ethylene Glycol (EOAc). Ethylene glycol (EG) was dried overnight under a high vacuum at 60 °C. EG (1 equiv) and an excess amount of tert-butyl acetoacetate (tBA, 4 equiv) were added to a 100 mL round-bottom flask. The mixture was stirred at room temperature until it became homogeneous. The viscous mixture was refluxed overnight at 130 °C under a nitrogen environment. After high reaction conversion was confirmed using thin layer chromatography (TLC), an excess amount of tBA and byproduct (tert-butanol) was continuously removed by purging nitrogen at 130 °C overnight. The crude product was purified by using medium-pressure liquid chromatography with a mixed solvent (diethyl ether and acetone). The ratio of eluents was adjusted, depending on the products. The final product was obtained as a yellow viscous liquid after drying overnight under high vacuum at 60 °C. The ¹H and ¹³C NMR spectra are shown in Figure S1.

Dynamic Network Synthesis. Acetylated EG monomers (EOAc, 1.5 equiv) were weighed into a 4 mL vial. LiTFSI salt (ratio between lithium salt and ethylene oxide:  $r = \frac{[\text{Li}^+]}{[\text{EO}]} = 0.033$  and 0.067 for 12EO and 0.1 for all vitrimers) was added to the vial. After the addition of 2 mL of THF into the vial, the mixture was sonicated for 15 min. Tris(2-aminoethyl)amine (TEA, 1 equiv) was then added into the vial and rigorously mixed using a vortex mixer for 20 s. The concentrations of all components in solutions are between 350 and 400 mg/mL. The solution was transferred quickly to a glass dish, and the resulting mixture was cured at 35 °C for 1 h and at 80 °C for 2 h under N<sub>2</sub> environment to remove solvent and minimize side reactions. The polymer network was further dried overnight at 130 °C under high vacuum to remove water and cure completely, resulting in yellow/orange polymer films. Subsequently, all samples were stored in a glovebox before further characterization. The as-synthesized vitrimers are named xEO-Neutral or xEO-LiTFSI, where x indicates the number of repeat units of ethylene oxide in EOAc. Neutral vitrimer networks were synthesized by the same procedure without adding salts.

VU Small-Molecule (tert-Butyl 3-Propylamino-2-buenoate) Synthesis for  $^7$ Li Solid-State NMR. A small VU molecule for  $^7$ Li solid-state NMR study was synthesized based on the literature. Propylamine (1.05 equiv) and 2.1 g of 4 molecular sieves were added to a 100 mL round-bottom flask with 6 mL of dichloromethane (DCM). Next, tert-butyl acetoacetate (1.00 equiv) was added. The mixture was then stirred at room temperature for 24 h and washed with dry DCM. After the solvent was evaporated, a light yellow liquid was obtained. The chemical structure was confirmed through  $^1$ H NMR (CDCl<sub>3</sub>, 500 MHz)  $\delta$  0.95 (t, 3H), 1.45 (s, 9H), 1.58 (m, 2H), 1.87 (s, 3H), 3.13 (td, 2H), 4.36 (s, 1H), 8.48 (s, 1H).

**ATR-FTIR.** Infrared spectra were obtained using a Bruker  $\alpha$  FT-IR spectrometer with a platinum-ATR QuickSnap sampling module. All samples were measured at 100 °C (above  $T_{\rm g}$ ) to ensure good contact between samples and window. The range of scanning is from 4000 to 400 cm<sup>-1</sup> with 32 scans and 4 cm<sup>-1</sup> resolution.

**Solution-Phase NMR.**  $^{1}\mathrm{H}$  and  $^{13}\mathrm{C}$  NMR spectra were obtained on a CB 500 MHz NMR spectrometer using CDCl $_{3}$  as the reference solvent.

**7Li Solid-State NMR.** <sup>7</sup>Li NMR spectra were obtained by using a Varian Unity Inova 300 MHz spectrometer. Samples were densely packed inside 4 mm ceramic rotors in a glovebox, and measurements were at a magic angle spinning (MAS) speed of 10 kHz with 5000 total scans. MNOVA software was used to determine chemical shifts and assign peaks of the collected spectra. For Li-VU, *r* is defined as the ratio of [small VU molecule] to [EO].

<sup>13</sup>C Solid-State NMR. A Carver B500 Bruker Avance III HD 500 MHz spectrometer was used to obtain <sup>13</sup>C solid-state NMR spectra of vitrimers. Samples were prepared by densely packing into a 6 mm ceramic rotor under inert conditions. The rotor is then spun at a magic angle spinning (MAS) speed of 8 kHz with direct polarization (DP) mode.

**DFT Simulations.** DFT calculations were performed with the Vienna ab initio Simulation Package (VASP). We use the generalizedgradient approximation to exchange and correlation, as parametrized by Perdew, Burke, and Ernzerhof (PBE) for all calculations.<sup>61</sup> The Brillouin zone is sampled at the  $\Gamma$ -point only, and the plane-wave expansion of the Kohn-Sham states is cut off at 400 eV. This converges the total energy to within 1 meV per atom. Simulation cells were constructed as follows: a cross-linking site is linked to a vinylogous urethane on all three branches. Two branches are terminated by a methyl group to simplify the calculation. The remaining branch is the N-EO branch. N EO repeat units are used for the PEO chain, with N = 2, 4, or 6. The opposing end of the PEO chain is terminated with a vinylogous urethane. SMILES representations of all structures are available in the SI. Rotated "cage" structures of 6-EO were constructed by the manual rotation of bond angles. The cell geometry for N-PEO structures was optimized by relaxing all atomic positions until forces on each atom were less than 0.025 eV  $Å^{-1}$ . The Li<sup>+</sup>-N-EO cells were constructed by adding a Li ion at each labeled site (Figure 4a) with a distance from the labeled atom of ~1.5 The cell geometry was optimized in a similar fashion, and the relaxations were stopped when the difference in the total energy for the Li+-N-EO cell between ionic relaxation steps was less than 1 meV. The ionized behavior was represented by reducing the number of electrons in the system by 1 during relaxation and calculation of the ground-state energy. Relaxed structures and the calculation output of all cells are available in the Materials Data Facility. 62,63,64 The binding energy,  $E_{\rm be}$ , of the Li ion is defined by the following equation:

$$E_{\rm be} = E_{\rm mol-Li} - E_{\rm mol} - E_{\rm Li}^{\phantom{\rm th}}$$

where  $E_{\rm mol-Li}$  is the ground-state energy of the relaxed Li<sup>+</sup>-N-PEO cell,  $E_{\rm mol}$  is the ground-state energy of the relaxed N-PEO cell, and  $E_{\rm Li}^+$  is the ground-state energy of an isolated Li<sup>+</sup> ion in vacuum. <sup>65</sup> Calculated ground-state energies for all reference and relaxed cells are provided in Table S1.

**Differential Scanning Calorimetry (DSC).** DSC measurements were performed on a TA Instruments DSC 2500. Samples weighing between 2 and 5 mg were sealed in Tzero aluminum pans inside a glovebox. Subsequently, the samples were subjected to a heat/cool/

heat cycle in a temperature range from -60 to  $120~^{\circ}\text{C}$  with  $10~^{\circ}\text{C}/\text{min}$  for all samples except 12EO networks, which were measured from -100 to  $120~^{\circ}\text{C}$  at the same rate. The glass transition temperature  $T_{\rm g}$  was determined using the  $1/2~\Delta C_{\rm p}$  criterion from the second heating cycle.

**Thermogravimetric Analysis (TGA).** The thermal stability of the polymer samples was assessed on a TA Instruments Q50. Each sample was heated from 30 to 600 °C at a rate of 10 °C/min under  $N_2$ . The isothermal experiments under  $N_2$  and air were performed at 130 °C for 2 h to confirm the elimination of water.

**Electrochemical Impedance Spectroscopy (EIS).** Impedance measurements were performed using a Bio-Logic SP300 potentiostat with a Controlled Environment Sample Holder and Intermediate Temperature System accessories. Impedance spectra were collected by applying an AC potential of 20 mV from 1 MHz to 100 mHz. The real conductivity ( $\sigma'$ ) was calculated from complex impedance,  $Z^* = Z' + i\omega Z''$  based on the equation

$$\sigma'(\omega) = \frac{1}{A} \times \frac{Z'(\omega)}{[Z'(w)^2 + Z''(w)^2]}$$

where l is the thickness of the film, A is the film surface area, and  $\omega$  is the frequency. All samples were prepared with CR2032 coin cells that were assembled following a previous literature protocol.  $^{24}$  Temperature-dependent impedance measurements were performed from 130 to 35 °C with 10 °C steps after reaching thermal equilibrium state at the highest temperature.

Transference measurements were performed with a Bio-Logic SP200 potentiostat. Circular disks from network samples were punched out of films and maintained at >100 °C under vacuum (≤50 mbar) overnight before testing. Li/Li symmetric cells were prepared by placing sample disks between two lithium foils with two layers of Kapton tape (thickness  $\sim$ 50  $\mu$ m) as the spacer to prevent shortage. The cell was hermetically sealed using a crimper in a glovebox. Coin cells were maintained in an iso-temperature oven set at a specific temperature (as noted) during measurement. Transference measurements were performed following a procedure in the literature: 66 cells were charged (1 h) and discharged (1 h) with current 5  $\mu$ A/cm<sup>2</sup>, repeated 6 times to generate a stable interface between the polymer and lithium before measurement (Figure \$15a): after 30 min, impedance spectra (1 MHz to1 Hz) were obtained with  $\Delta V = 20$  mV. Next,  $\Delta V = 40$  mV was applied to the cell and current was recorded for 2 h to generate a steady current  $I_{ss}$ , and then polarization impedance spectra (1 MHz to 1 Hz) were immediately measured with an amplitude of 20 mV. The transference number was

calculated via  $t^+ = \frac{I_{ss}}{I_\Omega} \left( \frac{\Delta V - I_\Omega R_0}{\Delta V - I_{ss} R_{ss}} \right)$ , where  $R_0$  is the initial interfacial resistance,  $R_s$  is the interfacial resistance when  $I_{ss}$  is reached,  $R_T$  is the total initial cell resistance, and  $R_T = R_{b0} + R_0$ ,  $R_{b0}$  is the impedance of bulk polymer.  $R_0$ ,  $R_{b0}$ , and  $R_{ss}$  were obtained by fitting impedance spectra to an equivalent circuit R + L + R1/Q1 + R2/Q2 (Figure

spectra to an equivalent circuit R + L + S15c,d). Results are shown in Table S3.

Rheology. Rheological characterization experiments were performed by using a TA Instruments DHR-2 rheometer outfitted with an environmental control chamber and 8 mm stainless-steel parallel plates. Prior to each measurement, samples were prepared into a circular geometry of 8 mm diameter using a stainless-steel mold at 130 °C by applying 3 tons for 15 min. Only the 2EO samples were hot-pressed at 150 °C for 30 min with the same pressure due to their longer relaxation time  $\tau^*$ . The samples were then loaded onto the rheometer plates preheated at 130 °C. Neutral vitrimer samples were measured without reprocessing, and it was confirmed that there were no observable bubbles or cracks in the samples prior to measurement. For the neutral vitrimer samples, the stress relaxation curve was processed with a smoothing function in the TRIOS rheometer software, which resulted in no significant change in the characteristic stress relaxation time. The thickness of disk samples ranged between 800 to 900  $\mu$ m. Stress relaxation experiments were then conducted at 10 °C intervals from 130 to 70 °C with applied strains of 0.5% for 2EO samples and 1% for all other samples. Temperature ramps were

(a)

$$HO \longleftrightarrow O_n^{\mathsf{H}} + O \longleftrightarrow O_n^{\mathsf{H}}$$

Figure 1. (a) Synthetic scheme for vinylogous urethane (VU) vitrimers, including ethylene oxide linkers and added LiTFSI salts. Acetoacetate groups are installed as terminal groups on PEG linkers, and reaction with tris(2-aminoethyl)amine forms a precise, telechelic VU network. (b) Proposed mechanism of Li-ion-catalyzed vinylogous urethane exchange. Li-ion coordination can activate carbonyl group and stabilize the zwitterionic intermediate.

performed by heating from 70 to 130 °C at a rate of 2 °C/min at 0.5 Hz. Dynamic oscillatory linear viscoelastic (LVE) experiments were measured from 100 to 0.05 rad/s at 130 C. All experiments were collected in the linear regime based on strain sweep measurements from 0.1 to 1.5% for 2EO samples and 0.1–5% for other samples at each temperature. Characteristic relaxation times were defined as the time where normalized modulus  $G(t)/G_o$  equals I/e. These relaxation times were plotted as a function of 1000 T and fit to an Arrhenius equation. The activation energy for the flow was determined in each sample from the slope.

**Reprocessing.** Vitrimer networks were first cut into small pieces (<3 mm) for reprocessing. Cut samples were then hot-pressed in a stainless-steel mold with an 8 mm diameter under the pressure of 3 tons at 130 °C or 150 °C on a Carver Hydraulic Unit Model 3912. After 15 or 30 min, the homogeneous film was carefully removed from the mold and quickly transferred to an argon glovebox. All reprocessed samples were stored under inert condition to prevent any side reaction or water adsorption.

## ■ RESULTS AND DISCUSSION

Vitrimers were synthesized by first converting ethylene glycols (xEGs, x=2, 3, 4, 6, 12) into telechelic acetoacetates in the presence of excess *tert*-butyl acetoacetate (tBAc). After detecting the desired product using TLC, excess tBAc and the byproduct tert-butanol were removed by heating at 130 °C under a dynamic nitrogen purge (Figure 1). Acetoacetate functionality was calculated based on peak integration from <sup>1</sup>H NMR for use in stoichiometry calculations (Figure S1). All acetoacetate functionalized ethylene oxides (EOAc) exhibit a high conversion of the alcohols. Next, neutral and ionic vinylogous urethane (VU) vitrimers were synthesized with

various lengths of EOAc. Conversion of the vitrimers was first confirmed using ATR-FTIR through the disappearance of the characteristic peaks of acetoacetate at 1711 and 1738 cm<sup>-1</sup> and the appearance of the characteristic peaks of VU at 1645 and 1590 cm<sup>-1</sup> (Figure S2).<sup>2,4</sup> In addition, thermal gravimetric analysis (TGA) was performed to determine the degradation temperatures and to quantitatively confirm the complete elimination of water during the polymerization. Any unreacted functional groups would also produce water when heated, and thus, TGA provides a second metric of high conversion. Each sample was heated from 30 to 600 °C under N<sub>2</sub> atmosphere at a rate of 10 °C/min. The degradation temperatures  $T_{\rm d,95\%}$  were found to be in good agreement with the values reported in the literature (Figure S3).<sup>48,53,54,59,60</sup>

The glass transition temperature  $T_{\rm g}$  of the vitrimers was determined by using differential scanning calorimetry (DSC) (Figure S4). In general,  $T_{\rm g}$  increases with increasing cross-linking density due to the suppression of chain mobility (Table 1), similar to prior reports. As discussed below, the  $T_{\rm g}$  difference between 2EO and 12EO vitrimers is significant (~88 °C) and must be taken into account when analyzing viscoelasticity and conductivity behavior. The addition of Li salts resulted in further increases in  $T_{\rm g}$  relative to the neutral networks, consistent with prior reports in other salt-loaded polymeric systems. As the concentration of Li increases, interactions between Li ions and ether oxygens in EO restrict the segmental dynamics. After investigating the effect of Li salt concentrations on ion conductivity and rheological behaviors of 12EO vitrimers (Figures S17 and S18, Table S4),

Table 1. Summary of Thermal and Viscoelastic Characteristics of Vinylogous Urethane Vitrimers<sup>a</sup>

samples	$T_{\rm g}$ (°C)	$T_{\rm d}$ (°C)	$ au_{130~^{\circ}\mathrm{C}}~(\mathrm{min})$	$E_{\rm a}$ (kJ/mol)
2EO-neutral	62	265.4		
2EO-LiTFSI	67	246.5	68.8	$91.8 \pm 11.2$
3EO-neutral	38	270.6		
3EO-LiTFSI	46	249.2	28.7	$87.9 \pm 4.0$
4EO-neutral	19	273.5		
4EO-LiTFSI	28	245.2	15.3	$93.1 \pm 9.3$
6EO-neutral	-2	277.6		
6EO-LiTFSI	17	261.0	10.1	$89.2 \pm 6.7$
12EO-neutral	-35	309.0	32.7	
12EO-LiTFSI	-21	294.7	0.47	$87.5 \pm 2.9$

 $<sup>^</sup>a\tau_{130~^\circ\text{C}}$  of all neutral vitrimers (except 12EO-Neutral) cannot be obtained within the experimental time scale because of slow exchange dynamics.

the ratio between lithium salt and ethylene oxide (defined as  $r = \frac{[\text{Li}^+]}{[\text{EO}]}$ ) was fixed at r = 0.1 for all vitrimers to understand how other parameters such as linker length and dynamic bond content impacts conductivity and rheology. Stress relaxation experiments of vitrimers with three different compositions confirm that the characteristic relaxation time of the vitrimer  $(\text{VU}_{1.00})$  occurs between two samples  $(\text{VU-EA}_{1.05})$  and  $(\text{VU-DA}_{0.95})$ , as shown in Figure S5.

The viscoelastic properties of VU vitrimers were studied as a function of linker length and salt addition (Figure 2). Both LiTFSI-containing and neutral vitrimers exhibit full stress relaxation (Figure 2a), unlike conventional thermosets with

static cross-links. However, the characteristic relaxation time  $\tau^*$ of 12EO-LiTFSI decreased by a factor of  $\sim$ 70 compared to the 12EO-Neutral sample (Figure S6), which is attributed to the catalytic effect of lithium ions that act as a Lewis acid. Higher levels of Li salt loading lead to lower activation energies for dynamic bond exchange in an Arrhenius plot of 12EO-LiTFSI as a function of salt concentration (Figure S18 and Table S4), revealing the catalytic effect of Li salts. The Li-ion catalyzed vinylogous urethane exchange mechanism is proposed in Figure 1b.<sup>22</sup> Non-normalized stress relaxation curves are shown in Figure S7. The stress relaxation plateau modulus (evaluated at time t = 1.015 s) for the 12EO vitrimer decreased upon adding more lithium salts compared to neutral vitrimer, which is attributed to the plasticizing effect of anions.<sup>48</sup> <sup>13</sup>C magic angle spinning (MAS) solid-state NMR spectrum of 12EO-LiTFSI provided qualitative evidence that the reaction is completed. In addition, salt addition does not hinder the elimination of water during the reaction, as confirmed by isothermal TGA at curing temperatures of 12EO-LiTFSI for 2 h (Figure S8). The temperature-dependent viscoelasticity of vitrimers was also investigated by measuring stress relaxation as a function of temperature. Faster stress relaxation was observed at higher temperatures, as dynamic bond exchange occurs more rapidly due to the higher thermal energy to overcome the energy barrier (Figure 2b).

To understand the effect of cross-linking density on the viscoelastic behavior of VU vitrimers, the stress relaxation time of LiTFSI vitrimers was characterized as a function of temperature (Figure 2c). The characteristic relaxation time of vitrimers shows a single temperature dependence over this window indicating the entire regime is controlled by a single

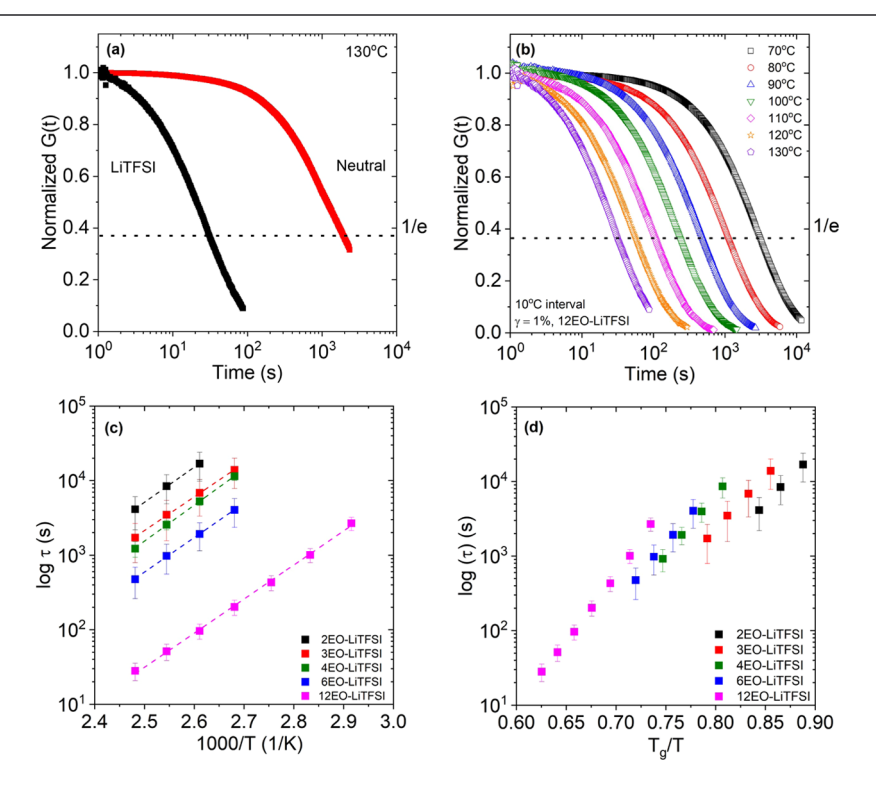


Figure 2. Representative stress relaxation experiments and Arrhenius plots of VU vitrimers. (a) Stress relaxation curves of 12EO-Neutral (black) and LiTFSI (red). The dotted line indicates  $G/G_0 = 1/e$ , which is used to define a characteristic relaxation time  $\tau^*$ . (b) Stress relaxation curves of 12EO-LiTFSI for the temperature window between 70 and 130 °C. (c) Arrhenius plot of the characteristic relaxation time as a function of the inverse temperature with various linker lengths. (d) Arrhenius plot of the characteristic relaxation time as a function of the inverse temperature normalized by the glass transition temperature  $T_e$ .

Table 2. Summary of the Viscoelastic Properties of Vinylogous Urethane Vitrimers with Salts<sup>b</sup>

samples	relaxation modulus (MPa) <sup>a</sup>	$M_{\rm c}$ (kg/mol)	cross-linking density (mol/L)	$ au_{130~^{\circ}\mathrm{C}}~(\mathrm{min})$	$E_{\rm a}({\rm kJ/mol})$
2EO-LiTFSI	2.066	1.70	0.616	68.8	$91.8 \pm 11.2$
3EO-LiTFSI	2.088	1.68	0.623	28.7	$87.9 \pm 4.0$
4EO-LiTFSI	1.795	2.06	0.502	15.3	$93.1 \pm 9.3$
6EO-LiTFSI	1.358	2.98	0.347	10.1	$89.2 \pm 6.7$
12EO-LiTFSI	0.268	13.1	0.080	0.47	$87.5 \pm 2.9$

<sup>a</sup>Density is assumed to be 1.034 kg/mol for all samples. <sup>b</sup>Stress relaxation modulus G(t) was taken at time t = 1.015 s at 130 °C.

bond exchange mechanism. 5,6,56 Moreover, values of activation energy for the vitrimers ranged from 87 to 91 kJ/mol, which are in good agreement with prior work. 27,55 The densest network 2EO-LiTFSI shows the longest relaxation time due to the high cross-linking density, leading to restricted chain mobility and slower dynamic exchanges (Table 2). As the cross-linking density decreases, the stress relaxation times also decrease as previously observed in telechelic silicone, ethylene oxide, and ethylene vitrimers with boronic ester cross-links. 5,57,23,24,58 Literature on VU telechelic networks 22,52 showed an opposite trend which is thought to arise due to a substantially higher molecular weight between cross-links which alters the balance between dynamic bond sites and mobility. Characteristic relaxation times do not collapse onto a single universal curve for different linker lengths when plotted as a function of the normalized temperature  $T_{\rm g}/T$ , which suggests that their viscoelastic properties are decoupled from segmental dynamics (Figure 2d). Unlike conventional PEObased solid electrolytes, 41-44 all VU vitrimers preserved their modulus at high temperatures due to a conserved network topology (Figure S9).

To probe the local coordination environment,  $^7\text{Li}$  solid-state NMR (ssNMR) was performed on samples with the same  $r = [\text{Li}^+]/[\text{EO}] = 0.1$  ratios (Figure 3).  $^7\text{Li}$  ssNMR is often used to investigate the interaction between Li ions and dipoles along with polymer chains.  $^{67,72}$  Lithium can accelerate VU bond exchange and be solvated by ethylene oxide by coordinating with the ether oxygens.  $^{22}$  Here, Li-EO refers to a mixture of LiTFSI salts and diethylene glycol ethyl ether (DEG) that serves as a small-molecule PEG mimic. Li-VU refers to a

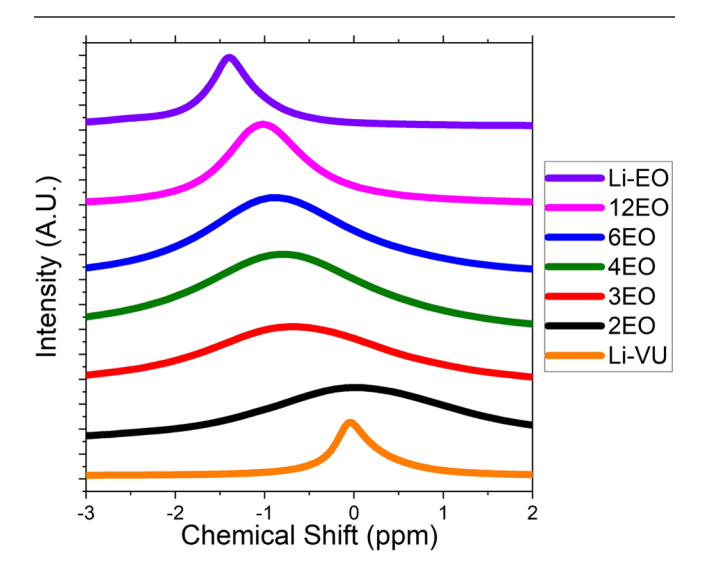
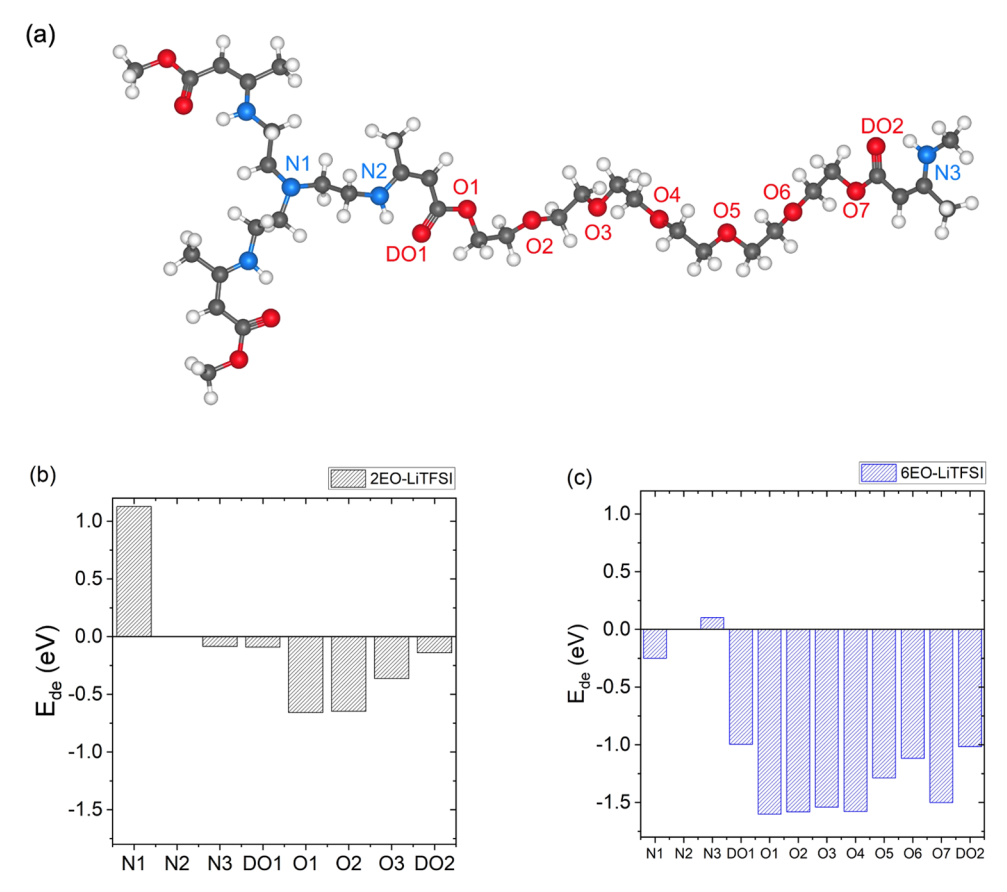


Figure 3. <sup>7</sup>Li solid-state NMR illustrating the effect of various linker lengths on coordination of Li<sup>+</sup> with ether oxygens and VU dynamic bond sites.

mixture of LiTFSI salts and a small-molecule VU compound without any EO functionality (Figure S10). Li-ion coordination with the VU dynamic bond and the EO backbone is detected at distinct wavenumbers and chemical shifts. In the FTIR spectra of the vitrimers, the vinylogous urethane peaks shift to lower wavenumbers (Figures S2 and S16) as Li ions coordinate with different sites along the VU backbone. In addition, the Li-ion coordination environment in the networks systematically changes as a function of the linker length (Figure 3). For longer linkers, ethylene glycol coordination with Li is preferred over coordination to the VU sites. PEObased polymer electrolytes generally require six ether oxygens to form stable coordination with lithium cations. 34,35 However, short linkers cannot effectively solvate Li, and instead the cation sits preferentially at the VU site, as clearly observed in the 2EO network. However, all vitrimers exhibit broader peaks compared to those of the two reference samples, which indicates a complex interplay of solvation sites in the polymer networks.

The interaction of Li ions with different sites along the VU backbones (O and N) was investigated using density functional theory (DFT) simulations (Figure 4). Simulation cells were composed of three branches of PEO chains. Two branches are terminated by a methyl group to simplify the calculation. The remaining branch is the N-PEO branch (N =2, 4, or 6) and is terminated by a VU (Figure 4a). Before the binding energy was calculated, all atomic positions were relaxed (see the Supporting Information). All binding energies of Li ions along different sites are summarized in Table S1. Delta binding energy  $(E_{de})$  is used to determine which site is more favored and stable compared to N1 at the dynamic bonding site. For both 2EO and 6EO systems, E<sub>de</sub> values of ether oxygen sites (O1-7) are lower than those of the dynamic bonding sites (N2, DO1, N3, DO2), confirming that Li-EO coordination is favored rather than Li-VU coordination (Figure 4b). In general, longer EO chains result in lower  $E_{de}$ , which is consistent with <sup>7</sup>Li ssNMR results where longer EO chains have peaks closer to the EO-VU reference peak (Figure 3).

The ionic conductivity of vitrimers with Li salts was measured using electrochemical impedance spectroscopy (EIS) over a broad temperature range (130 to 35 °C) as shown in Figure 5. The ionic conductivity of 12EO-LiTFSI at 35 °C is  $5.52 \times 10^{-6}$  S/cm. However, in the case of 2EO-LiTFSI, it can be measured above 65 °C due to its low conductivity. As cross-linking density increases, ionic conductivity decreases due to glass transition temperature ( $T_g$ ) effect (Figure 5a). Higher  $T_g$  impedes segmental dynamics of polymer chains, resulting in hindered ion transport. The ionic conductivity values at 70 °C are  $9.36 \times 10^{-5}$ ,  $3.94 \times 10^{-6}$ ,  $6.47 \times 10^{-7}$ ,  $7.71 \times 10^{-8}$  and,  $8.86 \times 10^{-9}$  S/cm, for samples 12EO, 6EO, 4EO, 3EO, and 2EO, respectively. It is worth noting that all samples are well described by the Vogel–Fulcher–Tamman (VFT) model (Table S2), which indicates



**Figure 4.** Density functional theory (DFT) reveals interactions between Li ions and binding sites. (a) Structure of a relaxed VU vitrimer in the presence of Li ions. (b, c) Plot of delta binding energy  $E_{de}$  of a Li ion with different binding sites, where  $E_{de}$  is calculated by subtracting the binding energy of each site from binding energy of N2.

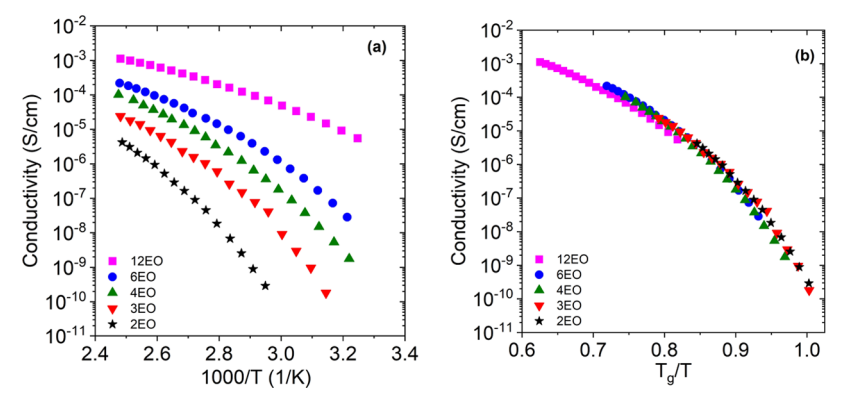


Figure 5. Ion transport in VU vitrimers. (a) Ionic conductivity as a function of inverse temperature for networks with different linker lengths. (b) Plot of  $T_{\rm g}$ -normalized temperature-dependent conductivities, revealing universal behavior indicating that ion transport is strongly coupled to polymer segmental dynamics.

coupling between segmental motion and ion transport in polymer electrolytes (Figure S11). However, there is no discernible trend among VFT fit parameters with the linker length or dynamic bond concentration. In order to understand the role of  $T_{\rm g}$  on conductivity, ionic conductivity for VU vitrimers is plotted against  $T_{\rm g}/T$  (Figure Sb). The data for all networks superimpose after normalizing the temperature by  $T_{\rm g}$  indicating that the chemical details of the solvation environment are not significant contributors to the conductivity. Despite the large difference ( $\sim$ 88 °C) in  $T_{\rm g}$  between 2EO (67 °C) and 12EO (-21 °C) vitrimers, ionic charge transport is primarily dominated by segmental dynamics in these networks.

The superposition of ionic conductivity is observed to be highly reproducible (Figure S12).

We further assessed the reprocessability and recyclability of EO-VU vitrimers for sustainable electrolyte applications (Figure 6). VU vitrimer samples were cut into small pieces and hot-pressed as described above (Methods section), except for the 2EO-LiTFSI samples, which were hot-pressed at 150 °C for 30 min with the same pressure due to the higher crosslinking density and  $T_{\rm g}$ . Only EO-LiTFSI samples can be reprocessed due to the catalytic effect of the lithium cations, <sup>22</sup> whereas the neutral networks are effectively intractable. Ionic vitrimer samples were able to be reshaped into homogeneous

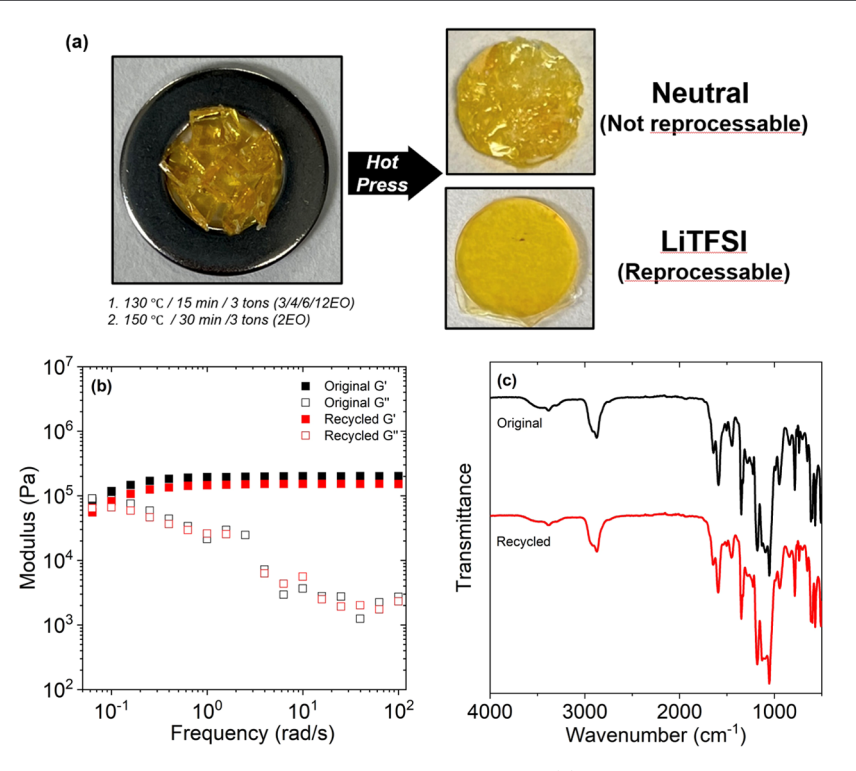


Figure 6. Demonstration of the reprocessability and recyclability of VU vitrimers. (a) Reprocessing of VU-Neutral and LiTFSI pieces into homogeneous films using a hot press. (b) Dynamic oscillatory linear viscoelastic (LVE) experiments and (c) FTIR data of 12EO-LiTFSI. These data illustrate that there is no significant degradation of dynamic bonds before and after recycling.

films by reprocessing. Dynamic oscillatory LVE experiments were performed to check for property variations after reprocessing and to determine the feasibility of recycling. As shown in Figure 6b, a slight decrease in the storage modulus plateau (0.20–0.15 MPa) was observed after the first recycling process. The change in mechanical properties can be attributed to moisture from the environment, which can be introduced during reprocessing under ambient conditions. ATR-FTIR spectra for samples before and after recycling were examined to assess changes in the functional groups. It is worth mentioning that the location of the peaks does not change, suggesting that there is no significant degradation of dynamic bonds (Figure 6c), consistent with no change in color.

# CONCLUSIONS

In this work, the competing effects of EG length and VU concentration on salt partitioning, ionic conductivity, and linear viscoelasticity were investigated for a series of precise VU vitrimers. Compared to neutral vitrimers, a characteristic relaxation time for VU vitrimers is accelerated by a factor of ~70 due to the catalytic effect of the LiTFSI salt. The crosslinking density of the vitrimers was controlled using different linker lengths, and stress relaxation times increased with higher cross-linking density and increasing  $T_{\rm g}$ . The characteristic relaxation times do not superimpose when normalized by  $T_{\rm g}$ suggesting that the viscoelastic behavior is partially decoupled from segmental dynamics. However, the ionic conductivity collapses onto a universal curve upon normalizing the temperature by  $T_g$ , which implies that ionic charge transport is strongly coupled to segmental dynamics. From this perspective, the different coupling behavior of viscoelastic and ionic conductivity properties with segmental dynamics can be utilized to independently tune the mechanical and ion

transport properties of vitrimer electrolytes. In addition, <sup>7</sup>Li ssNMR and DFT simulations indicate that Li ions prefer to coordinate with oxygens along with ethylene oxide chains rather than VU bond sites as the linker length increases, and the chains have a greater ability to solvate the cations. Reprocessability of the salt vitrimers was further demonstrated with the addition of salt using a hot press method, indicating the ability of these solid electrolytes to be recycled. Overall, this work provides new insights into the effect of salt addition and cross-linking density on the viscoelastic and ionic conductivity properties of VU vitrimers, which provides new avenues for controlling the mechanical and ion transport properties of recyclable solid polymer electrolytes.

# ASSOCIATED CONTENT

# **5** Supporting Information

The Supporting Information is available free of charge at https://pubs.acs.org/doi/10.1021/acs.chemmater.3c01353.

Solution/solid-state <sup>1</sup>H/<sup>13</sup>C NMR; FT-IR spectra; TGA; DSC; normazlied/non-normalized stress relaxation curves; rheological characterization of 2/3/4/6/12EO-LiTFSI as a function of temperature (stress relaxation, temperature sweep); ionic conductivity measured by EIS; DFT structures and delta binding energy as a function of sites; and Li<sup>+</sup> transference number measurements (PDF)

# AUTHOR INFORMATION

#### **Corresponding Authors**

Charles M. Schroeder – Department of Materials Science and Engineering, Beckman Institute for Advanced Science and Technology, and Department of Chemical and Biomolecular Engineering, University of Illinois at Urbana–Champaign,

Urbana, Illinois 61801, United States; Oorcid.org/0000-0001-6023-2274; Email: cms@illinois.edu

Christopher M. Evans — Department of Materials Science and Engineering, Materials Research Laboratory, Beckman Institute for Advanced Science and Technology, and Department of Chemical and Biomolecular Engineering, University of Illinois at Urbana—Champaign, Urbana, Illinois 61801, United States; orcid.org/0000-0003-0668-2500; Email: cme365@illinois.edu

#### **Authors**

- Seongon Jang Department of Materials Science and Engineering, Materials Research Laboratory, and Beckman Institute for Advanced Science and Technology, University of Illinois at Urbana—Champaign, Urbana, Illinois 61801, United States
- Erick I. Hernandez Alvarez Department of Materials Science and Engineering and Materials Research Laboratory, University of Illinois at Urbana—Champaign, Urbana, Illinois 61801, United States; orcid.org/0000-0001-5093-8089
- Chen Chen Department of Materials Science and Engineering, Materials Research Laboratory, and Beckman Institute for Advanced Science and Technology, University of Illinois at Urbana—Champaign, Urbana, Illinois 61801, United States; orcid.org/0000-0002-8926-9860
- Brian B. Jing Department of Materials Science and Engineering and Materials Research Laboratory, University of Illinois at Urbana—Champaign, Urbana, Illinois 61801, United States
- Chengtian Shen Department of Materials Science and Engineering and Materials Research Laboratory, University of Illinois at Urbana—Champaign, Urbana, Illinois 61801, United States
- Paul V. Braun Department of Materials Science and Engineering, Materials Research Laboratory, Beckman Institute for Advanced Science and Technology, and Department of Chemistry, University of Illinois at Urbana—Champaign, Urbana, Illinois 61801, United States; orcid.org/0000-0003-4079-8160
- André Schleife Department of Materials Science and Engineering, Materials Research Laboratory, and National Center for Supercomputing Applications, University of Illinois at Urbana—Champaign, Urbana, Illinois 61801, United States; orcid.org/0000-0003-0496-8214

Complete contact information is available at: https://pubs.acs.org/10.1021/acs.chemmater.3c01353

#### Notes

The authors declare no competing financial interest.

# ACKNOWLEDGMENTS

The authors gratefully acknowledge the use of research facilities at National Center for Supercomputing for Applications (for DFT calculations), Material Research Laboratory (for TGA and DSC), Beckman Institute for Advanced Science and Technology, and School of Chemical Sciences NMR Laboratory (for solution and solid-state NMR) at the University of Illinois at Urbana—Champaign. This project was supported by the Air Force Office of Scientific Research, Organic Materials Chemistry Program (grant FA 9550-20-1-0262, rheological analysis, and characterization), the National Science Foundation (NSF) via the Molecular Maker

Lab Institute (Award 201987, NSF AI Institute, molecular design), the DIGIMAT NRT (award 1922758, DFT simulations), the Department of Energy Basic Energy Sciences Materials Chemistry program (award DE-SC0020858, transference numbers), and the NSF GRFP (award DGE-1746047, to E.I.H.A.).

# **■** REFERENCES

- (1) Lebreton, L.; Andrady, A. Future scenarios of global plastic waste generation and disposal. *Palgrave Commun.* **2019**, *5* (1), No. 6.
- (2) Schneiderman, D. K.; Hillmyer, M. A. 50th Anniversary Perspective: There Is a Great Future in Sustainable Polymers. *Macromolecules* **2017**, *50* (10), 3733–3749.
- (3) Epps, T. H., III; Korley, L. T. J.; Yan, T.; Beers, K. L.; Burt, T. M. Sustainability of Synthetic Plastics: Considerations in Materials Life-Cycle Management. *JACS Au* **2022**, 2 (1), 3–11.
- (4) Montarnal, D.; Capelot, M.; Tournilhac, F.; Leibler, L. Silica-Like Malleable Materials from Permanent Organic Networks. *Science* **2011**, 334 (6058), 965–968.
- (5) Soman, B.; Evans, C. M. Effect of Precise Linker Length, Bond Density, and Broad Temperature Window on the Rheological Properties of Ethylene Vitrimers. *Soft Matter* **2021**, *17*, 3569–3577.
- (6) Porath, E.; Evans, C. M. Importance of Broad Temperature Windows and Multiple Rheological Approaches for Probing Viscoelasticity and Entropic Elasticity in Vitrimers. *Macromolecules* **2021**, *54* (10), 4782–4791.
- (7) Xie, D.-M.; Zhang, Y.-X.; Li, Y.; Beng, J.-B. Castor Oil-drived Sustainable Poly(urethane urea) Covalent Adaptable Networks with Tunable Mechanical Properties and Multiple Recyclability based on Reversible Piperdine-urea Bond. *Chem. Eng. J.* **2022**, 446, No. 137071, DOI: 10.1016/j.cej.2022.137071.
- (8) Taynton, P.; Zhu, C.; Loob, S.; Shoemaker, R.; Pritchard, J.; Jin, Y.; Zhang, W. Re-healable Polyimine Thermosets: Polymer Composition and Moisture Sensitivity. *Polym. Chem.* **2016**, *7*, 7052.
- (9) Zheng, N.; Fang, Z.; Zou, W.; Zhao, Q.; Xie, T. Thermoset Shape-memoery Polyurethane with Intrinsic Plasticity Enabled by Transcarbamoylation. *Angew. Chem., Int. Ed.* **2016**, *55*, 11421–11425.
- (10) Liu, H.; Zhang, H.; Wang, H.; Huang, X.; Huang, G.; Wu, J. Weldable, Malleable and Programmable Epoxy Vitrimers with High Mechanical Properties and Water Insensitivity. *Chem. Eng. J.* **2019**, 368, 61–70.
- (11) Joe, J.; Shin, J.; Choi, Y.-S.; Hwang, J. H.; Kim, S. H.; Han, J.; Park, B.; Lee, W.; Park, S.; Kim, Y. S.; Kim, D.-G. A 4D Printable Shape Memory Vitrimer with Repairability and Recyclability through Network Architecture Tailoring from Commercial Poly( $\epsilon$ -caprolactone). *Adv. Sci.* **2021**, 8, No. 2103682, DOI: 10.1002/advs.202103682.
- (12) Denissen, W.; Baere, I. D.; Paepegem, W. V.; Leibler, L.; Winne, J.; Du Prez, F. E. Vinylogous Urea Vitrimers and Their Application in Fiber Reinforced Composites. *Macromolecules* **2018**, *51*, 2054–2064, DOI: 10.1021/acs.macromol.7b02407.
- (13) Liu, Y. Y.; He, J.; Li, Y. D.; Zhao, X. L.; Zeng, J. B. Biobased Epoxy Vitrimer from Epoxidized Soybean Oil for Reprocessable and Recyclable Carbon Fiber Reinforced Composite. *Compos. Commun.* **2022**, 22, No. 100445, DOI: 10.1016/j.coco.2020.100445.
- (14) Xu, Y.; Dai, S.; Bi, L.; Jiang, J.; Zhang, H.; Chen, Y. Catalyst-free Self-healing Bio-based Vitrimer for a Recyclable, Reprocessable, and Self-adhered Carbon Fiber Reinforced Composite. *Chem. Eng. J.* **2022**, *429*, No. 132518, DOI: 10.1016/j.cej.2021.132518.
- (15) Hubbard, A. M.; Ren, Y.; Papaioannou, P.; Sarvestani, A.; Picu, C. R.; Konkolewicz, D.; Roy, A. K.; Varshney, V.; Nepal, D. Vitrimer Composites: Understanding the Role of Filler in Vitrimer Applicability. *ACS Appl. Polym. Mater.* **2022**, *4* (9), 6374–6385.
- (16) Lee, J.; Jing, B. B.; Porath, L. E.; Sottos, N. R.; Evans, C. M. Shock Wave Energy Dissipation in Catalyst-Free Poly-(dimethylsiloxane) Vitrimers. *Macromolecules* **2020**, *53*, 4741–4747.

- (17) Whiteley, J. M.; Taynton, P.; Zhang, W.; Lee, S.-H. Ultra-thin Solid-State Li-Ion Electrolyte Membrane Facilitated by a Self-Healing Polymer Matrix. *Adv. Mater.* **2015**, *27*, 6922–6927.
- (18) Wan, L.; Cao, X.; Xue Xiaoyuan, X.; Tong, Y.; Ci, S.; Huang, H.; Zhou, D. Self-Healing and Flexible Ionic Gel Polymer Electrolyte Based on Reversible Bond for High-Performance Lithium Metal Batteries. *Energy Technol.* **2021**, *10*, No. 2100749, DOI: 10.1002/ente.202100749.
- (19) Cao, X.; Zhang, P.; Guo, N.; Tong, Y.; Xu, Q.; Zhou, D.; Feng, Z. Self-healing Solid Polymer Electrolyte based on Imine Bonds for High Safety and Stable Lithium Metal Batteries. *RSC Adv.* **2021**, *11*, 2985
- (20) Zhang, L.; Zhang, P.; Chang, C.; Guo, W.; Guo, H.; Pu, X. Self-Healing Solid Polymer Electrolyte for Room-Temperature Solid-State Lithium Metal Batteries. *ACS Appl. Mater. Interfaces* **2021**, *13*, 46794–46802.
- (21) Deng, K.; Zhou, S.; Xu, Z.; Xiao, M.; Meng, Y. A High Ion-conducting, Self-healing and Nonflammable Polymer Electrolyte with Dynamic Imine Bonds for Dendrite-free Lithium Metal Batteries. *Chem. Eng. J.* **2022**, 428, No. 131224.
- (22) Liu, Y.; Chen, Y.; Yu, Z.; Huang, Z.; Lai, J.-C.; Tok, J. B.-H.; Cui, Y.; Bao, Z. Reprocessable and Recyclable Polymer Network Electrolyte via Incorporation of Dynamic Covalent Bonds. *Chem. Mater.* **2022**, 34 (5), 2393–2399, DOI: 10.1021/acs.chemmater.1c04396.
- (23) Jing, B. B.; Mata, P.; Zhao, Q.; Evans, C. M. Effects of Crosslinking Density and Lewis Acidic Sites on Conductivity and Viscoelasticity of Dynamic Network Electrolytes. *J. Polym. Sci.* **2021**, *59*, 2492–2501.
- (24) Jing, B. B.; Evans, C. M. Catalyst-free Dynamic Networks for Recyclable, Self-healing Solid Polymer Electrolytes. *J. Am. Chem. Soc.* **2019**, *141* (48), 18932–18937.
- (25) Denissen, W.; Rivero, G.; Nicolay, R.; Leibler, L.; Winne, J. M.; Du Prez, F. E. Vinylogous Urethane Vitrimer. *Adv. Funct. Mater.* **2015**, 25, 2451–2457.
- (26) Taplan, C.; Guerre, M.; Winne, J. M.; Du Prez, F. E. Fast Processing of Highly Crosslinked, Low-Viscosity Vitrimers. *Mater. Horiz.* **2020**, *7*, 104–110.
- (27) Denissen, W.; Droesbeke, M.; Nicolay, R.; Leibler, L.; Winne, J. M.; Du Prez, F. E. Chemical Control of the Viscoelastic Properties of Vinylogous Urethane Vitrimers. *Nat. Commun.* **2017**, *8*, No. 14857.
- (28) Rosso, M.; Gobron, T.; Brissot, C.; Chazalviel, J. N.; Lascaud, S. Onset of Dendritic Growth in Lithium/Polymer Cells. *J. Power Sources* **2001**, 97–98, 804–806.
- (29) Dolle, M.; Sannier, L.; Beaudoin, B.; Trentin, M.; Tarascon, J. M. Live Scanning Electron Microscope Observations of Dendritic Growth in Lithium/Polymer Cells. *Electrochem. Solid-State Lett.* **2002**, *5*, A286–A289.
- (30) Li, W. Y.; Yao, H. B.; Yan, K.; Zheng, G. Y.; Liang, Z.; Chiang, Y. M.; Cui, Y. The Synergetic Effect of Lithium Polysulfide and Lithium Nitrate to Prevent Lithium Dendrite Growth. *Nat. Commun.* **2015**, *6*, No. 7436, DOI: 10.1038/ncomms8436.
- (31) Lopez, J.; Mackanic, D. G.; Cui, Y.; Bao, Z. N. Designing Polymers for Advanced Battery Chemistries. *Nat. Rev. Mater.* **2019**, 4 (5), 312–330.
- (32) Zhao, Q.; Stalin, S.; Zhao, C.-Z.; Archer, L. A. Designing Solid-State Electrolytes for Safe, Energy-Dense Batteries. *Nat. Rev. Mater.* **2020**, 5 (3), 229–252.
- (33) Li, J.; Cai, Y.; Wu, H.; Yu, Z.; Yan, X.; Zhang, Q.; Gao, T. Z.; Liu, K.; Jia, X.; Bao, Z. Polymers in Lithium-Ion and Lithium Metal Batteries. *Adv. Energy Mater.* **2021**, *11* (15), No. 2003239, DOI: 10.1002/aenm.202003239.
- (34) Fenton, D. E.; Parker, J. M.; Wright, P. V. Complexes of Alkali-Metal Ions with Poly(Ethylene Oxide). *Polymer* 1973, 14, 589.
- (35) Shriver, D. F.; Papke, B. L.; Ratner, M. A.; Dupon, R.; Wong, T.; Brodwin, M. Structure and Ion-Transport in Polymer-Salt Complexes. *Solid State Ionics* **1981**, *5*, 83–88.
- (36) Dupon, R.; Papke, B. L.; Ratner, M. A.; Shriver, D. F. Ion-Transport in the Polymer Electrolytes Formed Between Poly-

- (Ethylene Succinate) and Lithium Tetrafluoroborate. *J. Electrochem. Soc.* 1984, 131, 586–589.
- (37) Gadjourova, Z.; Andreev, Y. G.; Tunstall, D. P.; Bruce, P. G. Ionic Conductivity in Crystalline Polymer Electrolytes. *Nature* **2001**, 412, 520–523.
- (38) Pandy, A.; Mullin, S.; Gomez, E. D.; Wanakule, N.; Chen, V. L.; Hexemer, A.; Pople, J.; Balsara, N. P. Effect of Molecular Weight and Salt Concentration on Conductivity of Block Copolymer Electrolytes. *Macromolecules* **2009**, 42, 4632–4637, DOI: 10.1021/ma900451e.
- (39) Xue, Z. G.; He, D.; Xie, X. L. Poly(ethylene oxide)-based Electrolytes for Lithium-ion Batteries. *J. Mater. Chem. A* **2015**, 3, 19218–19253.
- (40) Webb, M. A.; Jung, Y.; Pesko, D. M.; Savoie, B. M.; Yamamoto, U.; Coastes, G. W.; Balsara, N. P.; Wang, Z. G.; Miller, T. F. 3rd Systematic Computational and Experimental Investigation of Lithium-Ion Transport Mechanism in Polyester-Based Polymer Electrolytes. *ACS Cent. Sci.* **2015**, *1* (4), 198–205, DOI: 10.1021/acscentsci.5b00195.
- (41) Shim, J.; Kim, D.-G.; Lee, J. H.; Baik, J. H.; Lee, J.-C. Synthesis and properties of organic/inorganic hybrid branched-graft copolymers and their application to solid-state electrolytes for high-temperature lithium-ion batteries. *Polym. Chem.* **2014**, *5*, 3432–3442, DOI: 10.1039/C4PY00123K.
- (42) Zardalidis, G.; Ioannou, E.; Pispas, S.; Floudas, G. Relating Structure, Viscoelasticity, and Local Mobility to Conductivity in PEO/LiTf Electrolytes. *Macromolecules* **2013**, *46*, 2705–2714.
- (43) Zardalidis, G.; Gatsolui, K.; Pispas, S.; Mezger, M.; Floudas, G. Ionic Conductivity, Self-Assembly, and Viscoelasticity in Poly-(styrene-b-ethylene oxide) Electrolytes Doped with LiTf. *Macromolecules* **2015**, 48, 7164–7171, DOI: 10.1021/acs.macromol.5b01596.
- (44) Pipertzis, A.; Kafetzi, M.; Giaouzi, D.; Pispas, S.; Floudas, A. G. Grafted Copolymer Electrolytes Based on the Poly(acrylic acid-cooligo ethylene glycol acrylate) (P(AA-co-OEGA)) Ion-Conducting and Mechanically Robust Block. *ACS Apply. Polym. Mater.* **2022**, 7, 7070–7080, DOI: 10.1021/acsapm.2c00987.
- (45) Khurana, R.; Schaefer, J. L.; Archer, L. A.; Coates, G. W. Suppression of Lithium Dendrite Growth Using Cross-Linked Polyethylene/Poly(ethylene oxide) Electrolytes: A New Approach for Practical Lithium-Metal Polymer Batteries. J. Am. Chem. Soc. 2014, 136, 7395–7402.
- (46) Lu, Q.; He, Y.-B.; Yu, Q.; Li, B.; Janeti, Y. V.; Yao, Y.; Kang, F.; Yang, Q.-H. Dendrite-Free, High-Rate, Long-Life Lithium Metal Batteries with a 3D Cross-Linked Network Polymer Electrolyte. *Adv. Mater.* **2017**, 29, No. 1604460, DOI: 10.1002/adma.201604460.
- (47) Zhou, C.; Birney, D. M. Experimental and Theoretical Studies of the Dimerizations of Imidoylketenes. *J. Org. Chem.* **2004**, *69* (1), 86–94.
- (48) Liu, J.; Li, J.-J.; Luo, Z.-H.; Zhou, Y.-N. Fast room-temperature self-healing vitrimer enabled by accelerated associative exchange kinetics. *Chem. Eng. J.* **2023**, 452, No. 139452.
- (49) Pandy, A.; Mullin, S.; Gomez, E. D.; Chen, V. L.; Hexemer, A.; Pople, J.; Balsara, N. P. Effect of Molecular Weight and Salt Concentration on Conductivity of Block Copolymer Electrolytes. *Macromolecules* **2009**, 42, 4632–4637, DOI: 10.1021/ma900451e.
- (50) Chintapalli, M.; Thao, N. P.; Venkatesan, N. R.; Mackay, N. G.; Rojas, A. A.; Thelen, J. L.; Chen, C.; Devaux, D.; Balsara, N. P. Structure and Ionic Conductivity of Polystyrene-block-poly(ethylene oxide) Electrolytes in the High Salt Concentration Limit. *Macromolecules* **2016**, *49*, 1770–1780, DOI: 10.1021/acs.macromol.5b02620.
- (51) Inceoglu, S.; Rojas, A. A.; Devaux, D.; Chen, C.; Stone, G. M.; Balsara, N. P. Morphology-Conductivity Relationship of Single-Ion-Conducting Block Copolymer Electrolytes for Lithium Batteries. *ACS Macro Lett.* **2014**, *3*, 510–514.
- (52) Liu, J.; Li, J.-J.; Luo, Z.-H.; Zhou, Y.-N. Mapping Crosslinking Reaction-Structure-Property Relationship in Polyether-based Vinylogous Urethane Vitrimers. *AIChE J.* **2022**, *68*, No. e17578, DOI: 10.1002/aic.17587.

- (53) Spiesschaert, Y.; Taplan, C.; Stricker, L.; Guerre, M.; Winne, J. M.; Du Prez, F. E. Influence of the Polymer Matrix on the Viscoelastic Behaviour of Vitrimer. *Poly. Chem.* **2020**, *11* (33), 5377–5385.
- (54) Haida, P.; Abetz, V. Acid-Mediated Autocatalysis in Vinylogous Urethane Vitriemrs. *Macromol. Rapid Commun.* **2020**, 41, No. 2000273, DOI: 10.1002/marc.202000273.
- (55) Lijsebetten, F. V.; Brukcker, K. D.; Spiesschaert, Y.; Winne, J. M.; Du Prez, F. E. Suppressing Creep and Promoting Fast Reprocessing of Vitrimers with Reversibly Trapped Amines. *Angew. Chem., Int. Ed.* **2022**, *61*, No. e202113872, DOI: 10.1002/anie.202113872.
- (56) Hajj, R.; Duval, A.; Dhers, S.; Averous, L. Network Design to Control Polyimine Vitirmer Properties: Physical Versus Chemical Approach. *Macromolecules* **2020**, *53*, 3796–3805.
- (57) Porath, L.; Huang, J.; Ramlawi, N.; Derkaloustian, M.; Ewoldt, R. H.; Evans, C. M. Relaxation of Vitrimers with Kinetically Distinct Mixed Dynamic Bonds. *Macromolecules* **2022**, *55* (11), 4450–4458.
- (58) Soman, B.; Evans, C. M. Effect of Precise Linker Length, Bond Density, and Broad Temperature Window on the Rheological Properties of Ethylene Vitrimers. *Soft Matter* **2021**, *17*, 3569.
- (59) Mackanic, D. G.; Yan, X.; Zhang, Q.; Matsuhisa, N.; Yu, Z.; Jiang, Y.; Manika, T.; Yan, H.; Liu, K.; Chen, X.; Cui, Y.; Bao, Z. Decoupling of Mechanical Properties and Ionic Conductivity in Supramolecular Lithium Ion Conductors. *Nat. Commun.* **2019**, *10*, No. 5384, DOI: 10.1038/s41467-019-13362-4.
- (60) Tominaga, Y.; Yamazaki, K.; Nanthana, V. Effect of Anions on Lithium Ion Conduction in Poly(ethylene carbonate)-based Polymer Electrolytes. *J. Electrochem. Soc.* **2015**, *162*, A3133—A3136.
- (61) Gajdoš, M.; Hummer, K.; Kresse, G.; Furthmüller, J.; Bechstedt, F. Linear Optical Properteis in the Projector-Augmented Wave Methodology. *Phys. Rev. B* **2006**, *73*, No. 045112.
- (62) Jang, S.; Alvarez, E. I. H.; Chen, C.; Jing, B. B.; Shen, C.; Braun, P. V.; Schleife, A.; Schroeder, C. M.; Evans, C. M. Control of Lithium Salt Partitioning, Coordination, and Solvation in Vitrimer Electrolytes. *Materials Data Facility* **2023**, DOI: 10.18126/c9zx-r4gs.
- (63) Blaiszik, B.; Chard, K.; Pruyne, J.; Ananthakrishnan, R.; Tuecke, S.; Foster, I. The Materials Data Facility: Data Services to Advance Materials Science Research. *JOM* **2016**, *68*, 2045–2052.
- (64) Blaiszik, B.; Ward, L.; Schwarting, M.; Gaff, J.; Chard, R.; Pike, D.; Chard, K.; Foster, I. A Data Ecosystem to Support Machine Learning in Materials Science. MRS Communications 2019, 9, 1125—1133
- (65) Zhang, P.; Guo, W.; Guo, Z. H.; Ma, Y.; Gao, L.; Cong, Z.; Zhao, X. J.; Qiao, L.; Pu, X.; Wang, Z. L. Dynamically Crosslinked Dry Ion-Conducting Elastomers for Soft Iontronics. *Adv. Mater.* **2021**, 33, No. 2101396, DOI: 10.1002/adma.202101396.
- (66) Shah, D. B.; Olson, K. R.; Karny, A.; Mecham, S. J.; DeSimone, J. M.; Balsara, N. P. Effect of Anion Size on Conductivity and Transference Number of Perfluoroether Electrolytes with Lithium Salts. J. Electrochem. Soc. 2017, 164 (14), A3511–A3517.
- (67) Zhou, Q.; Ma, J.; Dong, S.; Li, X.; Cui, G. Intermolecular Chemistry in Solid Polymer Electrolytes for High-Energy-Density Lithium Batteries. *Adv. Mater.* **2019**, 31, No. 1902029, DOI: 10.1002/adma.201902029.
- (68) Lv, Z.; Tang, Y.; Dong, S.; Zhou, Q.; Cui, G. Polyurethane-based polymer elecytolytes for lithium Batteries: Advances and perspectives. *Chem. Eng. J.* **2022**, 430, No. 132659, DOI: 10.1016/j.cej.2021.132659.
- (69) Kato, R.; Mirmira, P.; Sookezian, A.; Grocke, G. L.; Patel, S. N.; Rowan, S. J. Ion-Conducting Dynamic Solid Polymer Electrolyte Adhesives. *ACS Macro. Lett.* **2020**, 9 (4), 500–506.
- (70) Jo, Y. H.; Li, S.; Zuo, C.; Zhang, Y.; Gan, H.; Li, S.; Yu, L.; He, D.; Xie, X.; Xue, Z. Self-Healing Solid Polymer Matrix for Lithium-Ion Batteries. *Macromolecules* **2020**, *53* (3), 1024–1032.
- (71) Wang, H.; Shi, Z.; Guo, K.; Wang, J.; Gong, C.; Xie, X.; Xue, Z. Boronic Ester Transesterification Accelerates Ion Conduction for Comb-like Solid Polymer Electrolytes. *Macromolecules* **2023**, *56* (6), 2494–2504.

- (72) Tominaga, Y. Ion-conductive polymer electrolytes based on poly(ethylene carbonate) and its derivatives. *Polym. J.* **2017**, *49*, 291–299
- (73) Zhao, Q.; Shen, C.; Halloran, K. P.; Evans, C. M. Effect of Network Architecture and Linker Polarity on Ion Aggregation and Conductivity in Precise Polymerized Ionic Liquids. *ACS Macro Lett.* **2019**, *8*, 658–663.
- (74) Sun, Z.; Wu, J.; Yuan, H.; Lan, J.; Yu, Y.; Zhu, Y.; Yang, X. Self-healing polymer electrolyte for long-life and recyclable lithium-metal batteries. *Materials Today Energy* **2022**, *24*, No. 100939.
- (75) He, Y.; Ma, M.; Li, L.; Zhao, S.; Zhao, X.; Advincula, R.; Tian, M.; Gao, S.; Yang, H.; Cao, P.-F. Hybrid Dynamic Covalent Network as a Protective Layer and Solid-State Polymer Electrolyte for Stable Lithium-Metal Batteries. *ACS Appl. Mater. Interfaces* **2023**, *15* (19), 23765–23776, DOI: 10.1021/acsami.3c02728.
- (76) Huang, Y.; Wang, J.; Shi, Z.; Wang, H.; Xue, Z. Disulfide bondembedded polyurethane solid polymer electrolytes with self-healing and shape-memory performance. *Polym. Chem.* **2022**, *13*, 6002.
- (77) Gu, W.; Li, F.; Liu, T.; Gong, S.; Gao, Q.; Li, J.; Fang, Z. Recyclable, Self-Healing Solid Polymer Electrolytes by Soy Protein-Based Dynamic Network. *Adv. Sci.* **2022**, *9*, No. 2103623, DOI: 10.1002/advs.202103623.
- (78) Xue, X.; Cao, X.; Wan, L.; Tong, Y.; Li, T.; Xie, Y. Crosslinked network solid polymer electrolyte with self-healing ability and high stability for lithium metal battery. *Polym. Int.* **2022**, *71*, 1201–1209.
- (79) Zhou, S.; Deng, K.; Xu, Z.; Xiao, M.; Meng, Y. Highly conductive self-healing polymer electrolytes based on synergetic dynamic bonds for highly safe lithium metal batteries. *Chem. Eng. J.* **2022**, *442*, No. 136083, DOI: 10.1016/j.cej.2022.136083.
- (80) Li, F.; Nguyen, G. T. M.; Vancaeyzeele, C.; Vidal, F.; Plesse, C. Healable Ionoelastomer Designed from Polymeric Ionic Liquid and Vitrimer Chemistry. ACS Appl. Polym. Mater. 2023, 5, 529–541.

